HHS Public Access

Author manuscript

J Control Release. Author manuscript; available in PMC 2016 December 28.

Published in final edited form as:

J Control Release. 2015 December 28; 220(0 0): 651–659. doi:10.1016/j.jconrel.2015.09.007.

Targeted delivery of platinum-taxane combination therapy in ovarian cancer

Swapnil S. Desale[a], **Kruti S. Soni**[a], **Svetlana Romanova**[a], **Samuel M. Cohen**[b], and **Tatiana K. Bronich**[a,*]

[a]Department of Pharmaceutical Sciences and Center for Drug Delivery and Nanomedicine, College of Pharmacy, University of Nebraska Medical Center, 985830 Nebraska Medical Center, Omaha, NE 68198-5830, USA

[b]Department of Pathology and Microbiology, University of Nebraska Medical Center, Omaha, Nebraska, 68198-3135, USA

Graphical abstract

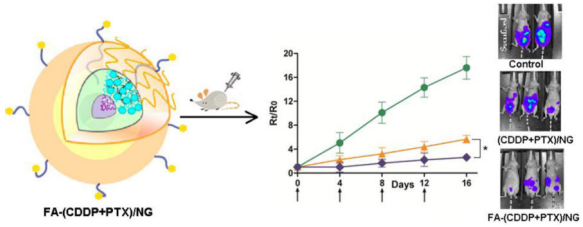

1. Introduction

Combination chemotherapy is preferred over treatment with single agents to combat most cancers as it targets multiple cell-survival pathways at the same time and delays the onset of resistance. This helps in achieving long-term tumor remission and increases median survival [1]. Cisplatin (CDDP)-based therapy has been the standard treatment for ovarian cancer since its discovery. After paclitaxel (PTX) was shown to be effective in ovarian cancer, multiple clinical trials studied the overall efficacy of CDDP and PTX and found significant benefit over the pre-existing treatments. Since then, this combination has been the treatment of choice for both early stage as well as advanced cases of ovarian cancer [2, 3]. However, administration of two different agents comes with the inconvenience of repeated or extended duration of drug infusion in patients. Moreover, the most extensively used conventional formulation of paclitaxel, Taxol®, utilizes Cremophor EL (polyethoxylated castor oil) that has been linked to significant toxicities including allergic, hypersensitivity and anaphylactic reactions during infusion that require premedication and prolonged peripheral neuropathy. Combining such drugs in one delivery carrier is therefore a well-suited and convenient

*Corresponding authors: TKB, Tel: (402) 559-9351, Fax: (402) 559-9365, tbronich@unmc.edu.

strategy for controlling the pharmacokinetics and co-delivery of the desired drug ratio *in vivo*, to maximize the therapeutic potency and minimize drug-associated toxicities.

Cross-linked nanogels have been found to be promising drug carriers to achieve this goal. Being mostly hydrophilic in nature, nanogels are highly biocompatible with a high loading capacity for guest molecules [4]. The nanogel structure can be readily adjusted to integrate features of different materials and, thus, offer advantages for combinatorial encapsulation of drugs with varying physicochemical properties. One of the widespread synthetic techniques for the synthesis of nanogels is the crosslinking of preformed coreshell self-assemblies such as polymer micelles that allows introducing a high degree of spatial organization into the nanogels [4, 5]. Cross-linking is known to impart control over the swelling behavior of the nanogels and thus helps in achieving controlled release of the incorporated cargo, which is an added advantage over the structural integrity imparted to the carrier system upon *in vivo* administration [4, 6]. The enhanced stability also makes the prolonged circulation of the nanogels possible, which in turn allows for increased drug accumulation at the target site [5–9].

We have previously described a biodegradable hybrid nanogel carrier system (NG) for the combination of CDDP and PTX for ovarian cancer therapy, which not only mitigated the toxicities associated with the use of free drugs but also improved treatment outcome [10]. However, our system relied solely on the enhanced permeation and retention (EPR) effect to facilitate the delivery of the drug combination to the tumor site [11]. Regardless of the importance and popularity of EPR effect-based drug delivery, this strategy has some limitations related to the inter- and intra-tumor heterogeneity, variations in the density as well as permeability of the tumor vasculature that can affect the accumulation of nanocarriers. One of the popular approaches to circumvent these problems is by surface-functionalization of the drug carrier with ligands that can target receptors with differential expression on the cancer cell surface, which helps in increasing the mean residence time of the delivery system at the tumor site and improving target cell uptake [12–15]. One such receptor of interest is the folate receptor (FR). Malignant cells, due to their high rate of cell division, have an increased requirement of folic acid (FA), since it is essential component of cell metabolism and DNA synthesis and repair. To fulfill this higher need of FA, FR is known to be over-expressed in a large number of malignant tissues, including ovarian cancer, compared to normal tissues with the exception of the kidney and choroid plexus [16, 17]. Furthermore, this receptor becomes accessible via the plasma compartment only after the cells lose their polarity owing to malignant transformation which makes it a differential target for cancer tissue that is easily accessible for intravenously administered FA conjugated systems. Its natural ligand, FA, comes with the advantages of high binding affinity, stability and a simple chemical structure together with ease of availability, making it a suitable targeting ligand for ovarian cancer therapy. FA can thus be successfully conjugated to macromolecular systems without loss of binding affinity to its receptor [18]. Many different agents targeting the folate pathway are currently in clinical development [19]. To date, FA-targeted agents showed significant promise in phase II clinical trials but it has not been confirmed in phase III studies [20–22]. Accordingly, there is a need for further identification of new therapeutic combinations and refinement of patient selection. To this

end, FA-conjugated imaging agents could be used for pre-selection of patients based on the expression of FR [23] and several methods have been already developed for this purpose [24, 25].

Our group has previously demonstrated a tumor-specific delivery and improved anticancer effect *in vivo* of CDDP-loaded NGs decorated with FA targeting groups [26]. In the current study, we designed FA-linked NGs incorporating platinum-taxane combination, and examined whether FR-targeted concurrent delivery of synergistic combination of CDDP and PTX can lead to enhanced therapeutic efficacy compared to nontargeted NG system.

2. Materials and Methods

Materials

α-Amino-ω-methoxy poly(ethylene glycol) (mPEG-NH_2, Mw = 5000 g mol^{-1}, M_w/M_n = 1.05) was purchased from Creative PEGWorks Inc., (NC, USA). Fmoc-NH-PEG-NH_2 (M_w = 7500 g mol^{-1}, Mw/Mn = 1.04) was purchased from JenKem technology (TX, USA). CDDP was purchased from Acros Organics (NJ, USA). L-Glutamic acid γ-benzyl ester (BGlu), L-phenylalanine (Phe), 1,2-ethylenediamine (ED), 1-(3-dimethylaminopropyl)-3-ethylcarbodiimide hydrochloride (EDC), paclitaxel, folic acid and other chemicals were purchased from Sigma-Aldrich (MO, USA) and were used without further purification. Fetal bovine serum (FBS), RPMI 1640 medium, penicillin, streptomycin, Trypsin–ethylenediaminetetraacetic acid (EDTA) (0.5% trypsin, 5.3 mM EDTA tetra-sodium) and other chemicals were purchased from Invitrogen (CA, USA).

Preparation of polymeric NGs

Poly(ethylene glycol)-*b*-poly(L-glutamic acid)-*b*-poly(L-phenylalanine) block copolymer with 90:25 ratio of glutamic acid and phenylalanine units (PEG-$PGlu_{90}$-$PPhe_{25}$) was synthesized as previously described [10]. Details of the procedures used for polymer synthesis and characterization are described in the Supplementary Information. NGs were prepared by using previously described method [10] using PEG-$PGlu_{90}$-$PPhe_{25}$ micelles as templates for further cross-linking by ED and EDC ([EDC]/[ED] = 2; [COOH]/[EDC] = 5) at r.t., overnight. Byproducts of the cross-linking reaction were removed by exhaustive dialysis of the reaction mixtures against distilled water. To synthesize fluorescence (Alexa 594)-labeled NGs, solution of Alexa Fluor 594 hydrazide (0.25 μmol, equivalent to 1% of carboxylate groups in NGs) in DMF was added to aqueous dispersion of NGs and the mixture was incubated for 2 h in dark. Unbound dye was removed by filtration on Ultracon filter units (MWCO 10,000 Da, Millipore) at 3000 rpm for 15 min (3 washes) and then additionally purified using NAP-10 column (GE healthcare). Notably, the same stock of Alexa 594-labeled NGs was used to prepare FA-decorated NGs.

Synthesis of FA-decorated NGs and drug loading

FA targeting moieties were conjugated to drug-loaded NGs via PEG spacer having Fmoc protection group (Fmoc-NH-PEG-NH_2). Firstly, Fmoc-NH-PEG-NH_2 (0.013 mmol, 0.05 eq with respect to the amount of carboxylate groups and 1.5 eq with respect to required FA) was conjugated to the free carboxyl groups (0.25 mmol) of NGs via EDC (0.023 mmol)

chemistry. Fmoc group was then removed by adding 5 μL of 30% piperidine/DMF (1.1 eq piperidine, 0.014 mmol) and incubating the reaction mixture for 10 min. Resulting constructs were purified using repeated ultrafiltration (MWCO 30,000, Millipore) at 3000 rpm for 15 min (3 washes). i e exclusion chromatography (ÄKTA Fast Protein Liquid Chromatography system) was used to determine the presence of residual PEG. PEG-NGs conjugates were analyzed by proton nuclear magnetic resonance spectroscopy (^{1}H NMR) using Varian INOVA 500 NMR spectrometer (Varian, Palo Alto, CA) operating at 500 MHz (1 mg/mL, D_2O, pH 7.0, 25 °C). The dispersion of PEG-conjugated NGs was mixed with an aqueous solution of CDDP (1mg/mL) at pH 9.0 at a 0.5 molar ratio of CDDP (0.12 mmol) to carboxylate groups (0.24 mmol) of the NGs followed by incubation at 37 °C for 48 h. Unbound CDDP was removed by Ultracon filter units (MWCO 10,000 Da, Millipore) at 3000 rpm for 15 min. FA (0.025 mmol) dissolved in water was subsequently reacted with 1.5 eq EDC (0.037 mmol) at pH 7 for 2 h. This EDC-activated FA was then conjugated to amine terminus of the PEG linker. Amount of FA was selected based on the previously reported optimal density of FA on NGs (0.1–0.2 μmol/mg of polymer) to maintain good loading, stability and cell uptake [26]. The amount of conjugated FA was determined by UV spectrometry (ε_{363}=6500 $M^{-1}cm^{-1}$) using non-modified PEG-conjugated NGs reference. Finally, PTX (0.01 mmol) was solubilized into the hydrophobic PPhe core of CDDP-loaded FA-modified NGs using an extraction method [27]. According to this method, a thin film of PTX (prepared by evaporation of a methanol solution of PTX) was incubated with aqueous dispersion of NGs (24 h, r.t.). Unincorporated PTX was removed by filtration with 0.8 μm syringe filters (Thermo Scientific). Similar procedures were used to prepare single drug NGs formulations. Pt content in NGs (Pt194/Pt195) was measured by the inductively coupled plasma-mass spectrometer (ICP-MS, NexION 300Q, ICP-MS spectrometer, PerkinElmer) calibrated with Pt (2–100 ng/ml) and Holmium as the internal standard. Samples were diluted in 1% HNO_3. PTX levels were determined by HPLC analysis under isocratic conditions using an Agilent 1200 HPLC system with a diode array detector set at 227 nm. As stationary phase a Nucleosil C18 column was used (250 mm × 4.6 mm), a mobile phase of acetonitrile/water mixture (55/45, v/v) was applied at a flow rate of 1 mL/min.

Physicochemical characterization of the NGs and drug release study

Intensity-mean Z-averaged particle diameter (D_{eff}) and ζ-potential of NGs were determined using a Zetasizer NanoZS (Malvern Instruments Ltd.). All measurements were performed in automatic mode at 25°C. Software provided by the manufacturer was used to calculate si e, polydispersity indices and ζ-potential of NGs. All measurements were performed at least in triplicate to calculate the mean values ± SD. Drug release from NGs was examined in PBS (pH 7.4, 0.14M NaCl) by dialysis method using a membrane with 3500 Da cutoff. The concentrations of Pt and PTX released were determined by ICP-MS and HPLC, respectively, and expressed as a percentage of the total Pt or PTX available vs. time.

Cell culture

A2780 human ovarian carcinoma cells were provided by Dr. P. Rogers (Institute of Cancer Research, University of Bristol, UK). A2780 cells were transfected using F-Luc-GFP Lentivirus (Capital Biosciences, Rockville, MD) according to manufacturer's protocol to obtain A2780/Luc cell line. Cells were cultured in folate-depleted RPMI 1640 medium (FD-

RPMI) with 2 mM glutamine, 10% (v/v) FBS, 100 U/ml penicillin and 0.1 mg/mL streptomycin at 37°C, 5% CO_2. This medium contains nearly physiological level of FA.

Flow cytometry and CDDP uptake

Cells (50,000 cells/well) grown in FD-RPMI media in 24-well plates for 2 days were exposed to Alexa 594-labeled NGs or FA-NG (0.20 μmol FA/mg of polymer) at 37°C for up to 2 h, washed three times with PBS, trypsinized, centrifuged (1500 rpm, 5 min) and re-suspended in PBS (pH 7.4). The % gated cells were analyzed using Becton Dickinson FACStarPlus flow cytometer and FACSDiva software (Version 8.0, Becton Dickinson, San Jose, CA). At least 5,000 events were acquired in linear mode, gated to exclude debris and dead cells, and visualized in logarithmic mode. For the competition assay, cells were co-incubated with Alexa 594-labeled FA-NGs in presence of free FA (25mM), and the experiment was carried out as described above.

In vitro cytotoxicity

A2780 cells seeded in 96-well plates (10,000 cells/well) 24 h before the experiment were exposed to various doses (0 –10 μg/ml on CDDP basis) of (CDDP+PTX)/NG or FA-(CDDP +PTX)/NG for 24 or 48 h in FD-RPMI at 37°C followed by washing with PBS, and maintaining in FD-RPMI medium with 10% FBS for additional 24 h. Cytotoxicity was determined by standard colorimetric MTT assay [28] and the IC_{50} values were calculated using GraphPad Prism Software. Ratio of CDDP to PTX was c.a. 10:1 (mol/mol).

Animals and bioluminescence imaging procedure

Female six-week old nude mice (athymic nude-nu) were obtained from Charles River Laboratories and housed in AAALAC accredited facility. Food and reverse osmosis water were available ad libitum throughout the study. Animals were quarantined for 7 days prior to study initiation. All animal studies were conducted in accordance with the protocol approved by the University of Nebraska Medical Center Institutional Animal Care and Use Committee. Imaging was conducted with the *in vivo* imaging system IVIS-200 (Xenogen Corporation, Alameda, CA) composed of a cooled charge-coupled device camera connected to a light-tight black chamber. Animals were maintained on a FA deficient diet (Harlan diet TD.00434) for a week before tumor inoculation and during the period of studies to achieve plasma folate levels in the physiologic range normally seen for humans [29]. Before *in vivo* imaging, animals were anesthetized with isoflurane (Henry Schein, Dublin, OH) and injected IP with D-luciferin (Perkin-Elmer, Waltham, MA) at the dose of 150 mg/kg (reconstituted in sterile PBS). Whole-body Imaging was performed 5 min after injection. Total bioluminescence signal in the regions of interest (ROIs) drawn around the whole abdomen region was quantified using Living Image software (version 2.50; Xenogen) and expressed as photons/s/cm^2/sr.

Animal studies

Peritoneal carcinomatosis was generated by IP injection of A2780/Luc cells (~1.75×10^6 cells). After development of tumors (3 days after injection) animals were randomized (8 treatment groups, n = 8) and treated with 5% dextrose (control) or free CDDP or (CDDP

+PTX)/NG or combination of CDDP/NG and PTX/NG at the same drug ratio or FA-(CDDP)/NG or combination of FA-(CDDP)/NG and FA-(PTX)/NG or FA-(CDDP +PTX)/NG or FA + FA-(CDDP+PTX)/NG at an equivalent dose of 4 mg/kg CDDP, or (4 mg/kg CDDP + 1 mg/kg PTX). Treatments were administered via tail vein injections at 4-day intervals. We used one additional group which received IP injection of FA-(CDDP +PTX)/NG. The treatment groups and the doses of each drug are presented in Table 1.

Animal body weight and tumor progression, as assessed by BLI, were monitored every fourth day. All images were acquired using identical BLI system settings. Tumors were allowed to grow until ascites developed or the mice showed signs of pain and/or distress, then the mice were euthanized via CO_2 asphyxiation. At necropsy, the abdominal cavity was carefully checked and the extent of tumor was determined.

Sample preparation and CDDP measurement in tissue

Known weights of thawed tissues (tumor, kidney, spleen, liver and lung), collected from the animals sacrificed at day 14 (2–3 mice per group) during treatment, were decomposed by wet-ashing in screw-capped vials with six volumes of concentrated nitric acid, overnight heating, and stirring at 65°C. An iridium internal standard was added prior to digestion. Total platinum concentrations were determined by ICP-MS using iridium correction. Calibration range for the assay was platinum 2–100 ng/mL with extrapolation to platinum 1000 ng/mL. Necessary dilutions were made when the platinum concentration exceeded the calibration range. Assay sensitivity was 0.8 ng of Pt/mL, with inter- and intraday assay variability not exceeding 5%.

Cancer antigen (CA)-125 assay and histopathology

Serum from the blood of sacrificed animals was collected and analyzed for CA-125 levels using CA-125 ELISA kit (Abcam, MA) according to t e manufacturer's instructions. Formalin-fixed tissues were processed, sectioned, inserted into tissue cassettes, dehydrated in 70% ethanol overnight, and paraffin embedded (UNMC Tissue Sciences Facility, Omaha, NE). Serial 5 μm sections were stained wit hematoxylin and eosin (H&E). For histopathological diagnosis, H&E-stained slides were examined by light microscopy and photomicrographs were taken using a Nikon camera mounted on a Nikon Eclipse 600 microscope (both Nikon Instruments, Melville, NY) with Adobe Elements 3.0 software (Adobe Systems, San Jose, CA).

Statistical analysis

Statistical comparisons for in vitro studies were carried out using Students *t*-test. In animal studies, group means BL signal intensity and body weights were analyzed using one-way analysis of variance [30]. Survival was estimated using Kaplan–Meier analysis and compared using log-rank test. *P* values less than 0.05 were considered significant. Analysis of variance and Kaplan–Meier analysis tests were performed using GraphPad Prism 5 (GraphPad Software, Inc.).

3. Results and Discussion

Preparation and characterization of folate-targeted NGs

Triblock copolymer PEG-$PGlu_{90}$-$PPhe_{25}$ was utilized for the synthesis of multi-compartment biodegradable NG. We have previously demonstrated that the incorporation of Phe moieties into PEG-PGlu block copolymers facilitated self-assembly of block copolymers in an aqueous medium, w ic was ascribed to ydrop obic and π-π stacking interactions of t e p enylalanine units, and was essential for solubili ation of various hydrophobic compounds [10, 27]. As it was reported, the incorporation of aromatic units in the polymer chains forming the hydrophobic micellar core can considerably improve the stability, loading capacity and drug retention of taxane-loaded polymeric micelles [31–34]. These favorable properties were attributed to π-π stacking and hydrophobic interactions between aromatic groups in t e micelle's core, and those of the drug. Therefore, we believe that PPhe domains in our NG system may provide a suitable environment for encapsulation of PTX. NGs were prepared as previously described by template-assisted method involving self-assembly of these amphiphilic block copolymers into micelles, followed by chemical cross-linking of the polyion chains [10]. The cross-linking was achieved via condensation reactions between the carboxylic groups of PGlu segments and the amine groups of ethylenediamine in the presence of a water-soluble carbodiimide. The resulting NGs displayed an average diameter of about 90 nm (ζ-potential = −20 mV) and were uniform (monomodal, narrow size distribution) as determined by dynamic light scattering (DLS). Such NGs have 1) a hydrophobic core formed by PPhe chains, which serves as a reservoir for PTX solubilization, 2) an anionic intermediate layer, which can incorporates CDDP through coordination with the carboxylic groups of PGlu, and 3) an outer PEG shell, which stabilizes NGs in aqueous dispersion. The crosslinks incorporated into PGlu block layer ensure that NGs remain stable until they encounter proteases, which degrade them by cleaving the polypeptide chains of the block copolymers [10]. NGs were further modified by FA via a PEG linker for delivering drug combination to FR-positive ovarian tumors. Scheme for the preparation of FA-targeted nanogels is presented in Figure 1.

To this end, EDC activated NGs were first reacted with Fmoc-NH-PEG-NH_2 (we chose PEG with a longer chain length, Mw = 7.5 kDa, to reduce steric interference with receptor binding) followed by deprotection of Fmoc groups. The deprotection was confirmed by disappearance of Fmoc signals in PEG-NGs ^{1}H NMR spectrum (Fig. S1). The hydrodynamic diameter of PEGylated NGs was 94 ± 3 nm, which is only slightly larger t an t at of precursor NGs (88 ± 2 nm). However, t e ζ-potential of the PEG-modified NGs significantly increased to −11.1 ± 2.5 mV compared to −20.0 ± 1.2 mV for the unmodified NGs (Table S2), which can be indicative of consumption of the PGlu carboxylate groups that reacted with the PEG linkers as well as additional shielding of surface charge by tethered PEG chains. Finally, EDC-activated FA was reacted to amino groups on NG-attached PEG linkers. Conjugation using carbodiimide chemistry is known to produce inactive α- and active γ-isomers of folate. However, since multiple folate residues were linked to each nanogel, the resulting FA-NGs contained sufficient amounts of t e active γ-derivative as shown in the cell association studies described below. After thorough purification, little to no residual PEG or FA was present in the final FA-NGs as was

confirmed by size exclusion chromatography (Fig. S2). The particle size and ζ-potential of FA-NGs remained practically the same as those of the PEGylated NGs (Table S2).

We have previously shown that the attachment of the FA groups should be carried out after NGs loading with CDDP to avoid inactivation of folate through CDDP binding with its carboxylic groups [26]. Therefore, in this study to prepare targeted NGs with binary drug combination (further abbreviated as FA-(CDDP+PTX)/NGs), CDDP was first loaded into PEGylated NGs followed by conjugation of FA ligands to PEG linkers. At the next step, PTX was solubilized into targeted CDDP/NGs using an extraction method. FA-(CDDP +PTX)/NG were small particles (D_{eff} of approximately 95 nm) with unimodal particle size distribution (PDI = 0.24) and contained 0.2 μmol FA per mg of polymer. As expected, the net negative charge of drug-loaded NGs was further decreased (ζ-potential = −5 mV) as a result of neutralization of PGlu segments upon CDDP binding. The average weight ratio of the CDDP and PTX incorporated into NGs was about 4 : 1, which has been previously shown to provide strong synergistic cytotoxic effects [10]. A similar procedure was used to prepare nontargeted (CDDP+PTX)/NGs from PEGylated NG precursors. Notably, the drug content and physicochemical characteristics of targeted FA-(CDDP+PTX)/NGs were quite similar to nontargeted NGs (Table 2). Moreover, FA-(CDDP+PTX)/NG were stable in aqueous dispersions, exhibiting no aggregation or precipitation for a prolonged period of time (weeks) (Table 2). We have previously showed that such NG system can retain drug cargo for longer period of time (weeks) [10]

For both drugs there was very little difference in the release profiles between targeted FA-(CDDP+PTX)/NG and nontargted (CDDP+PTX)/NG, which indicates that the modification of nanogels with targeting groups had no influence on drug retention (Fig. 2). As it seen in Fig. 2, sustained but temporally distinct release of Pt [35] species and PTX was observed. Notably, PTX release was much faster than that of Pt [35], which is expected since PTX is physically entrapped into the PPhe core.

Cellular association and in vitro cytotoxicity of FA-NGs

To demonstrate effect of attachment of FA on cellular association of NGs, we used FR+ human ovarian carcinoma A2780 cells and FR− A549 lung carcinoma cells [26]. Cultured cells were treated with fluorescence Alexa 594-labeled FA-NGs or NGs for 30 min at 37°C. Particle association with cells was determined by flow cytometry. As expected, the cellular association of FA-NGs with FR+ cells significantly ($P < 0.01$) exceeded that of the nontargeted NG (Fig. 3). On the other hand, no difference in association of targeted and nontargeted NGs was observed with A549 cells (Fig. 3).

To further elucidate whether the enhanced cellular association of FA-NGs depends on specific binding to FR on the cell surface, A2780 cells were treated with FA-NGs in the presence of excess free FA (25 mM). Flow cytometry analysis revealed that the cellular association of FA-NGs was suppressed to the level of the nontargeted NGs (Fig. 3). This inhibition was also significant ($P < 0.05$) after 1 h of treatment in the FR+ A2780 cells (Fig. S3). These results validate that the conjugation of FA to the surface of NGs resulted in efficient and specific association with FR+ cells. It is worth noting that after two hours of treatment there was no significance between FR-targeted and nontargeted NGs uptake,

which internalized efficiently (approx. 90% gated cells) in both cell types (Fig. S3), indicating that a long incubation time could enhance non-specific uptake of NGs. These differences in cellular association translated into cytotoxicity (Table 3). The cytotoxicity of FA-(CDDP+PTX)/NG against FR+ A2780 cells was increased by two fold compared to (CDDP+PTX)/NG (IC_{50} expressed in CDDP equivalents: 1.4 ± 0.75 μM vs 3 ± 1.3 μM) at 24 h. Notably, t e difference between targeted and nontargeted formulations was only apparent at lower time point and it becomes negligible at 48 h.

Antitumor activity in intrapertoneal xenograft model

Our previous studies have shown effective tumor inhibition by platinum-taxane-loaded NG system in subcutaneously growing ovarian tumor model. Herein, we tested the efficacy and the toxicity of FR-targeted combination therapy in peritoneal xenograft model that mimics the clinical manifestations in the advanced stage of the human ovarian carcinomatosis. The A2780/luc cells, injected into the peritoneum of female nude mice, grew rapidly *in vivo* and were able to trigger formation of tumor nodules throughout the abdominal peritoneum that were detectable by BLI as early as 3 days post inoculation. If mice were left untreated, the bioluminescene signal rapidly increased and mice ultimately developed ascites in 2–3 weeks. Treatments were initiated on 4^{th} day post A2780/luc inoculation. IV administrations of each formulation were given 4 times at 4-day intervals at 4mg/kg CDDP and 1 mg/kg PTX equivalents per dose. CDDP (4 mg/kg) was also used as a control-free drug with the same dosing schedule. As shown in Fig. 4, all treatments were effective in delaying tumor progression in comparison with control group. Tumor growth inhibition ratio between treated versus control groups (T/C value) was calculated on day 16 after treatment initiation according to the formula: $T/C = (R_t - R_o)_{\text{treated tumor}} / (R_t - R_o)$ control tumor, where R_t and R_o represent the mean bioluminescence intensity on the evaluation day and at the start of the treatment, respectively (Table S3). Consistent with our previous observations [10], platinum-taxane combination administered as single NG formulation, (CDDP+PTX)/NG, was found to be significantly more effective (T/C= 0.26) than CDDP alone (T/C = 0.56, $P < 0.05$, Fig. S4). In contrast, the mice treated with a cocktail of single drug NG formulations (CDDP/NG + PTX/NG) at the same drug ratio had a similar impact on the tumor progression as free CDDP (Fig. S4). These data reinforce our hypothesis that synchronized delivery of platinum-taxane combination chemotherapy using NGs plays an essential role in its cytotoxic activity.

Tumor growth in the mice treated with (CDDP+PTX)/NG was further suppressed when the same drug combination was administered in FA-decorated NGs. FA− (CDDP+PTX)/NG showed significant tumor reduction as measured by BLI (T/C = 0.09) compared to nontargeted (CDDP+PTX)/NG group (T/C = 0.26, $P < 0.05$) (Fig 4A and 4B). As a result, combination therapy with FA-(CDDP+PTX)/NG significantly increased the probability of survival compared to its nontargeted counterpart (Fig. 4C). The median survival times (post-tumor inoculation) for the FA-(CDDP+PTX)/NG and (CDDP+PTX)/NG groups were 41 and 31 days, respectively ($P < 0.01$) (Table S3). Notably, the enhanced antitumor effect of FA-(CDDP+PTX)/NG was inhibited when it was administered with free FA (Fig 4A and 4B) suggesting that FA-decorated (CDDP+PTX)/NG display folate specificity and exhibit elevated activity through a mechanism involving *in vivo* FR. The peritoneal cavity is the

principal site of disease in ovarian cancer. The concept of direct IP administration of chemotherapy, especially to treat microscopic residual disease after debulking surgery, has been evaluated in many clinical trials and has demonstrated an improvement in overall and disease-free survival [2, 36, 37]. A randomized phase III clinical trial showed IP administration of CDDP and PTX plus IV PTX improves survival when compared to standard of care with IV combination of CDDP and PTX [2]. However, IP chemotherapy also led to significantly higher toxicities due to exposure of both cancer and healthy tissues to high concentrations of drugs. We, therefore, utilized our FA-(CDDP+PTX)/NG formulation to determine whether there are therapeutic advantages in providing targeted IP chemotherapy in ovarian cancer. As seen in Fig. 3B the BLI data shows a trend towards enhanced therapeutic efficacy of FA-(CDDP+PTX)/NG when administered IP (T/C = 0.05) compared to IV regimen (T/C = 0.09). Kaplan-Mayer survival analysis also demonstrated that mice given IP FA-(CDDP+PTX)/NG appear to have the best outcomes. However, the differences between groups were not statistically significant.

CA-125 also known as MUC16 is a protein that in humans is encoded by the MUC16 gene [38]. Around 90% of women with advanced ovarian cancer have elevated levels of CA-125 in their blood serum, making CA-125 a useful tool for detecting ovarian cancer after the onset of symptoms [39]. Monitoring CA-125 blood serum levels is also useful for determining how ovarian cancer is responding to treatment and for predicting a patient's prognosis after treatment [40]. It has frequently been used as an indicator of tumor progression in various ovarian cancer mouse xenograft models [41–43]. To further characterize tumor response to the treatments, we analyzed the serum CA-125 levels in mice on day 14 (second day after last injection). As shown in Fig. 5, levels of CA-125 were significantly low in the mice that received (CDDP+PTX)/NG compared to either control group ($P < 0.01$) or free CDDP group ($P < 0.05$). CA-125 levels were lowest in the mice that received FA-(CDDP+PTX)/NG either IV or IP. Notably, compared to nontargeted (CDDP+PTX)/NG group, IP treatment with FA-(CDDP+PTX)/NG resulted in significant decrease in serum CA-125 levels ($P< 0.05$) indicating its better therapeutic potential.

To compare the ability of the NGs-based carriers to deliver a cytotoxic payload to the tumor sites, we sacrificed 2–3 mice on day 14 and excised the tumors for CDDP content estimation. Both targeted and nontargeted drug-loaded NGs displayed enhanced tumor accumulation relative to administration of free drug supporting the well-known characteristic of nanoparticles to improve tumor drug delivery by the EPR effect (Fig. 6). However, FA-(CDDP+PTX)/NG induced a significantly higher Pt accumulation in the target site compared to nontargeted (CDDP+PTX)/NG ($P < 0.05$). This increase appeared to be due to FR-specific interaction of folated NGs with cancer cells because it was completely reversed by co-administration of free folate. We have previously showed that the average weight ratio of the CDDP and PTX in the tumors of the animals was same as the drug loading ratio in (CDDP+PTX)/NG, indicating the spatial–temporal synchronization of drug exposure. We expect the similar synchronized delivery of CDDP and PTX is occurred using our current NG systems as well. Notably, while all drug-loaded NGs displayed considerable accumulation of Pt in the highly perfused organs such as liver and spleen, tumor was the only tissue where Pt content was significantly higher for FA-(CDDP+PTX)/NG (Fig. 6).

FA-(CDDP+PTX)/NG treatment which was administered IP led to the maximum Pt retention in the tumors which may be a result of regional exposure to high drug concentrations at the tumor sites. This might be the reason for the observed enhanced tumor responsiveness with IP FA-(CDDP+PTX)/NG treatment. The binding of FA-(CDDP +PTX)/NG to and/or their uptake by FR+ cancer cells can retain them within the tumor for a longer period of time, prevent their rapid re-entering into systemic circulation and, thus, provide some benefits over passively targeted formulations. The introduction of FA moieties can also have an effect on pharmacokinetics and biodistribution of NGs and influence tumor uptake. Further detailed pharmacokinetic study may help to elucidate the relationship between the therapeutic effect of the FR-targeted NGs and distribution at the tumor and the whole body

To further determine whether concurrent targeted delivery of drug combination will have therapeutic benefits, we also compared the inhibition of tumor progression and survival between FA-(CDDP+PTX)/NG and a combination of targeted single drug formulations (FA-(CDDP)/NG + FA-(PTX)/NG) administered at the same drug ratio (Fig. 7 and S5). Our data showed significantly better tumor growth inhibition and survival for FA-(CDDP+PTX)/NG than FA-(CDDP)/NG + FA-(PTX)/NG. This confirms an advantage of delivering a platinum-taxane drug combination via single carrier to the same targeted cells simultaneously. We have not tested this strategy with other drug combinations. So at time we are not claiming that the same phenomena will hold true for other drug combinations.

Importantly, the introduction of targeting FA moieties on the surface of NGs did not alter the favorable toxicity profile of (CDDP+PTX)/NG formulation. Neither targeted nor nontargeted NG-based binary drug combination caused a significant change in body weight, indicating that the treatments were well tolerated (Fig. S6). In contrast, the same dose of free CDDP produced a considerable body weight loss (> 15%, $P < 0.05$), which indicated systemic toxicity of free CDDP (Fig. S6). In the kidney, the primary target organ of CDDP toxicity [44, 45], both targeted or nontargeted drug-loaded NGs showed significantly lower Pt levels than free CDDP (Fig. 6) which ameliorated CDDP-induced nephrotoxicity as confirmed by tissue histopathology analysis. Light microscopic examination of H&E stained kidney sections from sacrificed animals indicated focal tubular degeneration and regeneration in kidneys from all animals treated with free CDDP, while no histopathological changes were observed in kidney from animals in the FA-(CDDP+PTX)/NG-treated or (CDDP+PTX)/NG-treated groups compared with the control (Fig. S7). This is a significant result since a higher expression of FR in this organ may raise a concern of toxicity to this tissue [46]. We also observed focal acute inflammation in the lungs of animals treated with free CDDP while no such changes were detected in any of the NGs formulation (Fig. S5). Despite relatively higher exposure of liver and spleen to CDDP in the FA-(CDDP +PTX)/NG or (CDDP+PTX)/NG treatment, there was no evidence of liver or splenic toxicity by histopathology (Fig. S8). Mice which received FA-(CDDP+PTX)/NG IP also did not show any evidence of toxicity in any of the investigated organs. Indeed, the local delivery of FA-(CDDP+PTX)/NG into intraperitoneal cavity reduced nonspecific drug accumulation in normal tissues (spleen, liver, and kidney) (Fig. 5). Blood cell counting analysis on day 14 was conducted and normal cell counts were observed for red blood cells

and platelets for all groups (Table S4) while there was significant reduction in the count of white blood cells (below normal range) in the mice which were treated with free CDDP. In contrast, mice treated with drugs loaded in NGs did not have any changes in white blood cells compared to control (Fig. S8).

Collectively, these *in vivo* data support the efficacy of this targeted platinum-taxane combination therapy in FR-expressing ovarian cancer model without toxicity-related consequences.

4. Conclusion

In this study, we demonstrated that folate-decorated NGs carrying CDDP and PTX drug combination exerted enhanced antitumor efficacy, both in terms of tumor growth inhibition and survival, compared to its nontargeted counterpart in rapidly growing murine model of FR-positive ovarian cancer. This better efficacy was only observed when CDDP and PTX are concurrently delivered to the tumor sites. Our data also indicate that IP administration of FA-(CDDP+PTX)/NG can be more effective in the context of targeted combination therapy without extending its cytotoxicity to the normal tissues. Localized chemotherapy has demonstrated survival advantages in advanced ovarian cancer patients and our NG-based drug delivery system can be a suitable candidate for further optimization and pre-clinical evaluation of intraperitoneal chemotherapy for ovarian cancer.

Supplementary Material

Refer to Web version on PubMed Central for supplementary material.

Acknowledgments

We acknowledge the assistance of the Nanomaterials Core Facility of the Center for Biomedical Research Excellence (CoBRE), Nebraska Center for Nanomedicine supported by the Institutional Development Award from the National Institute of General Medical Sciences of the National Institutes of Health under grant number P20GM103480. We also thank the NMR and Flow Cytometry Core Facility (University of Nebraska Medical Center) and Lora Arnold for assistance in the histopathology review. The authors are grateful to Jinjin Zhang for help in the animal studies.

References

1. Jia J, Zhu F, Ma X, Cao ZW, Li YX, Chen YZ. Mechanisms of drug combinations: interaction and network perspectives. Nat Rev Drug Discov. 2009; 8:111–128. [PubMed: 19180105]
2. Armstrong DK, Bundy B, Wenzel L, Huang HQ, Baergen R, Lele S, Copeland LJ, Walker JL, Burger RA. Intraperitoneal cisplatin and paclitaxel in ovarian cancer. N Engl J Med. 2006; 354:34–43. [PubMed: 16394300]
3. Agarwal R, Kaye SB. Ovarian cancer: strategies for overcoming resistance to chemotherapy. Nat Rev Cancer. 2003; 3:502–516. [PubMed: 12835670]
4. Kabanov AV, Vinogradov SV. Nanogels as pharmaceutical carriers: finite networks of infinite capabilities. Angew Chem Int Ed Engl. 2009; 48:5418–5429. [PubMed: 19562807]
5. Talelli M, Barz M, Rijcken CJ, Kiessling F, Hennink WE, Lammers T. Core-crosslinked polymeric micelles: Principles, preparation, biomedical applications and clinical translation. Nano Today. 2015; 10:93–117. [PubMed: 25893004]

6. Rijcken CJ, Snel CJ, Schiffelers RM, van Nostrum CF, Hennink WE. Hydrolysable core-crosslinked thermosensitive polymeric micelles: synthesis, characterisation and in vivo studies. Biomaterials. 2007; 28:5581–5593. [PubMed: 17915312]
7. Peng J, Qi T, Liao J, Chu B, Yang Q, Li W, Qu Y, Luo F, Qian Z. Controlled release of cisplatin from pH-thermal dual responsive nanogels. Biomaterials. 2013; 34:8726–8740. [PubMed: 23948167]
8. Jin W, Xu P, Zhan Y, Shen Y, Van Kirk EA, Alexander B, Murdoch WJ, Liu L, Isaak DD. Degradable cisplatin-releasing core-s ell nanogels from witterionic poly (β-aminoester)-graft-PEG for cancer chemotherapy. Drug Deliv. 2007; 14:279–286. [PubMed: 17613015]
9. Liu P, Gou M, Yi T, Qi X, Xie C, Zhou S, Deng H, Wei Y, Zhao X. The enhanced antitumor effects of biodegradable cationic heparin-polyethyleneimine nanogels delivering HSulf-1 gene combined with cisplatin on ovarian cancer. Int J Oncol. 2012; 41:1504–1512. [PubMed: 22825572]
10. Desale SS, Cohen SM, Zhao Y, Kabanov AV, Bronich TK. Biodegradable hybrid polymer micelles for combination drug therapy in ovarian cancer. J Control Release. 2013; 171:339–348. [PubMed: 23665258]
11. Fang J, Nakamura H, Maeda H. The EPR effect: unique features of tumor blood vessels for drug delivery, factors involved, and limitations and augmentation of the effect. Adv Drug Deliv Rev. 2011; 63:136–151. [PubMed: 20441782]
12. Pattni, BS.; Torchilin, VP. Targeted Drug Delivery: Concepts and Design. Springer; 2015. Targeted Drug Delivery Systems: Strategies and Challenges; p. 3-38.
13. Danhier F, Feron O, Préat V. To exploit the tumor microenvironment: passive and active tumor targeting of nanocarriers for anti-cancer drug delivery. J Control Release. 2010; 148:135–146. [PubMed: 20797419]
14. Hong S, Leroueil PR, Majoros IJ, Orr BG, Baker JR, Banaszak Holl MM. The binding avidity of a nanoparticle-based multivalent targeted drug delivery platform. Chem Biol. 2007; 14:107–115. [PubMed: 17254956]
15. Talelli M, Rijcken CJ, Oliveira S, van der Meel R, en Henegouwen PMvB, Lammers T, van Nostrum CF, Storm G, Hennink WE. Reprint of " Nanobody—Shell functionalized thermosensitive core-crosslinked polymeric micelles for active drug targeting". Journal of Control Release. 2011; 153:93–102.
16. Wang Y, Zhao R, Russell RG, Goldman ID. Localization of the murine reduced folate carrier as assessed by immunohistochemical analysis. Biochim Biophys Acta. 2001; 1513:49–54. [PubMed: 11427193]
17. Desmoulin SK, Hou Z, Gangjee A, Matherly LH. The human proton-coupled folate transporter: Biology and therapeutic applications to cancer. Cancer Biol Ther. 2012; 13:1355–1373. [PubMed: 22954694]
18. Lu Y, Low PS. Folate-mediated delivery of macromolecular anticancer therapeutic agents. Adv Drug Deliv Rev. 2012; 64:342–352.
19. Vergote IB, Marth C, Coleman RL. Role of the folate receptor in ovarian cancer treatment: evidence, mechanism, and clinical implications. Cancer Metastasis Rev. 2015; 34:41–52. [PubMed: 25564455]
20. Naumann RW, Coleman RL, Burger RA, Sausville EA, Kutarska E, Ghamande SA, Gabrail NY, DePasquale SE, Nowara E, Gilbert L. PRECEDENT: a randomized phase II trial comparing vintafolide (EC145) and pegylated liposomal doxorubicin (PLD) in combination versus PLD alone in patients with platinum-resistant ovarian cancer. J Clin Oncol. 2013; 31:4400–4406. [PubMed: 24127448]
21. Morris R, Joyrich R, Naumann R, Shah N, Maurer A, Strauss H, Uszler J, Symanowski J, Ellis P, Harb W. Phase II study of treatment of advanced ovarian cancer with folate-receptor-targeted therapeutic (vintafolide) and companion SPECT-based imaging agent (99mTc-etarfolatide). Ann Oncol. 2014; 25:852–858. [PubMed: 24667717]
22. Vergote I, Armstrong D, Scambia G, Fujiwara K, Gorbunova V, Schweizer C, Weil S, Barnias A, Poole C, Sehouli J. Phase 3 double-blind, placebo-controlled study of weekly farletuzumab with carboplatin/taxane in subjects with platinum-sensitive ovarian cancer in first relapse. Int J Gynecol Cancer. 2013; 23(Supplement 1)

23. Sega EI, Low PS. Tumor detection using folate receptor-targeted imaging agents. Cancer Metastasis Rev. 2008; 27:655–664. [PubMed: 18523731]
24. Parker N, Turk MJ, Westrick E, Lewis JD, Low PS, Leamon CP. Folate receptor expression in carcinomas and normal tissues determined by a quantitative radioligand binding assay. Anal Biochem. 2005; 338:284–293. [PubMed: 15745749]
25. Fisher RE, Siegel BA, Edell SL, Oyesiku NM, Morgenstern DE, Messmann RA, Amato RJ. Exploratory study of 99mTc-EC20 imaging for identifying patients with folate receptor–positive solid tumors. J Nucl Med. 2008; 49:899–906. [PubMed: 18483093]
26. Nukolova NV, Oberoi HS, Cohen SM, Kabanov AV, Bronich TK. Folate-decorated nanogels for targeted therapy of ovarian cancer. Biomaterials. 2011; 32:5417–5426. [PubMed: 21536326]
27. Desale SS, Raja SM, Kim JO, Mohapatra B, Soni KS, Luan H, Williams SH, Bielecki TA, Feng D, Storck M. Polypeptide-based nanogels co-encapsulating a synergistic combination of doxorubicin with 17-AAG show potent anti-tumor activity in ErbB2-driven breast cancer models. J Control Release. 2015; 208:59–66. [PubMed: 25660204]
28. Ferrari M, Fornasiero MC, Isetta AM. MTT colorimetric assay for testing macrophage cytotoxic activity in vitro. J Immunol Methods. 1990; 131:165–172. [PubMed: 2391427]
29. Leamon CP, Reddy JA, Dorton R, Bloomfield A, Emsweller K, Parker N, Westrick E. Impact of high and low folate diets on tissue folate receptor levels and antitumor responses toward folate-drug conjugates. J Pharmacol Exp Ther. 2008; 327:918–925. [PubMed: 18791065]
30. Ferreira SA, Gama FM, Vilanova M. Polymeric nanogels as vaccine delivery systems. Nanomed Nanotechnol Biol Med. 2013; 9:159–173.
31. Shi Y, van Steenbergen MJ, Teunissen EA, Novo Ls, Gradmann S, Baldus M, van Nostrum CF, Hennink WE. Π–Π stacking increases t e stability and loading capacity of thermosensitive polymeric micelles for chemotherapeutic drugs. Biomacromolecules. 2013; 14:1826–1837. [PubMed: 23607866]
32. Shi Y, van der Meel R, Theek B, Oude Blenke E, Pieters EH, Fens MH, Ehling J, Schiffelers RM, Storm G, van Nostrum CF. Complete Regression of Xenograft umors upon argeted Delivery of Paclitaxel via Π–Π tacking tabilized Polymeric Micelles. ACS Nano. 2015; 9:3740–3752. [PubMed: 25831471]
33. Hamaguchi T, Matsumura Y, Suzuki M, Shimizu K, Goda R, Nakamura I, Nakatomi I, Yokoyama M, Kataoka K, Kakizoe T. NK105, a paclitaxel-incorporating micellar nanoparticle formulation, can extend in vivo antitumour activity and reduce the neurotoxicity of paclitaxel. Br J Cancer. 2005; 92:1240–1246. [PubMed: 15785749]
34. Logie J, McLaughlin CK, Tam RY, Shoichet MS. Innovative use of the taxol binding peptide overcomes key challenges of stable and high drug loading in polymeric nanomicelles. Chem Commun (Camb). 2015; 51:12000–12003. [PubMed: 26121243]
35. Chida N, Hirasawa Y, Ohkawa T, Ishii Y, Sudo Y, Tamura K, Mutoh S. Pharmacological profile of FR260330, a novel orally active inducible nitric oxide synthase inhibitor. Eur J Pharmacol. 2005; 509:71–76. [PubMed: 15713431]
36. Jaaback K, Johnson N. Intraperitoneal chemotherapy for the initial management of primary epithelial ovarian cancer. Cochrane Libr. 2006
37. Chan DL, Morris DL, Rao A, Chua TC. Intraperitoneal chemotherapy in ovarian cancer: a review of tolerance and efficacy. Cancer Manag Res. 2012; 4:413. [PubMed: 23226073]
38. Yin BW, Lloyd KO. Molecular Cloning of the CA125 Ovarian Cancer Antigen identification as a new mucin, MUC16. Journal of Biological Chemistry. 2001; 276:27371–27375. [PubMed: 11369781]
39. Gupta D, Lis CG. Pretreatment serum albumin as a predictor of cancer survival: a systematic review of the epidemiological literature. Nutr J. 2010; 9 10.1186.
40. Bast RC Jr, Klug TL, John ES, Jenison E, Niloff JM, Lazarus H, Berkowitz RS, Leavitt T, Griffiths CT, Parker L. A radioimmunoassay using a monoclonal antibody to monitor the course of epithelial ovarian cancer. N Engl J Med. 1983; 309:883–887. [PubMed: 6310399]
41. Shaw TJ, Senterman MK, Dawson K, Crane CA, Vanderhyden BC. Characterization of intraperitoneal, orthotopic, and metastatic xenograft models of human ovarian cancer. Mol Ther. 2004; 10:1032–1042. [PubMed: 15564135]

42. Burbridge MF, Kraus-Berthier L, Naze M, Pierre A, Atassi G, Guilbaud N. Biological and pharmacological characterisation of three models of human ovarian carcinoma established in nude mice: use of the CA125 tumour marker to predict antitumour activity. Int J Oncol. 1999; 15:1155–1217. [PubMed: 10568822]

43. Kraeber-Bodéré F, Mishra A, Thédrez P, Faivre-Chauvet A, Bardiès M, Imai S, Le Boterff J, Chatal J-F. Pharmacokinetics and biodistribution of samarium-153-labelled OC125 antibody coupled to CITCDTPA in a xenograft model of ovarian cancer. Eur J Nucl Med. 1996; 23:560–567. [PubMed: 8698062]

44. Uchino H, Matsumura Y, Negishi T, Koizumi F, Hayashi T, Honda T, Nishiyama N, Kataoka K, Naito S, Kakizoe T. Cisplatin-incorporating polymeric micelles (NC-6004) can reduce nephrotoxicity and neurotoxicity of cisplatin in rats. Br J Cancer. 2005; 93:678–687. [PubMed: 16222314]

45. Mizumura Y, Matsumura Y, Hamaguchi T, Nishiyama N, Kataoka K, Kawaguchi T, Hrushesky WJM, Moriyasu F, Kakizoe T. Cisplatin-incorporated polymeric micelles eliminate nephrotoxicity, while maintaining antitumor activity. Cancer Sci. 2001; 92:328–336.

46. Low PS, Henne WA, Doorneweerd DD. Discovery and development of folic-acid-based receptor targeting for imaging and therapy of cancer and inflammatory diseases. Acc Chem Res. 2007; 41:120–129. [PubMed: 17655275]

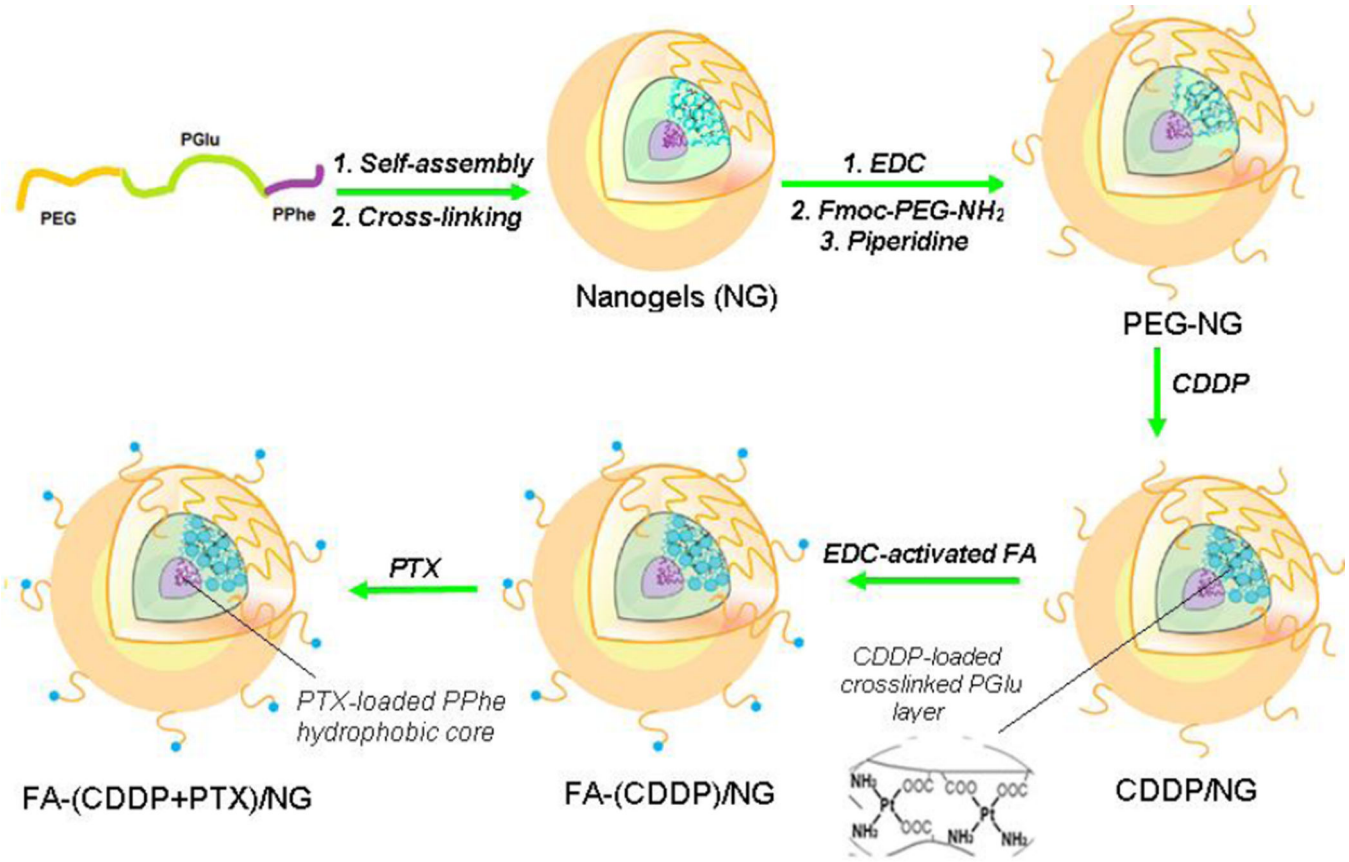

Figure 1.
Scheme for the preparation of FA-decorated NGs.

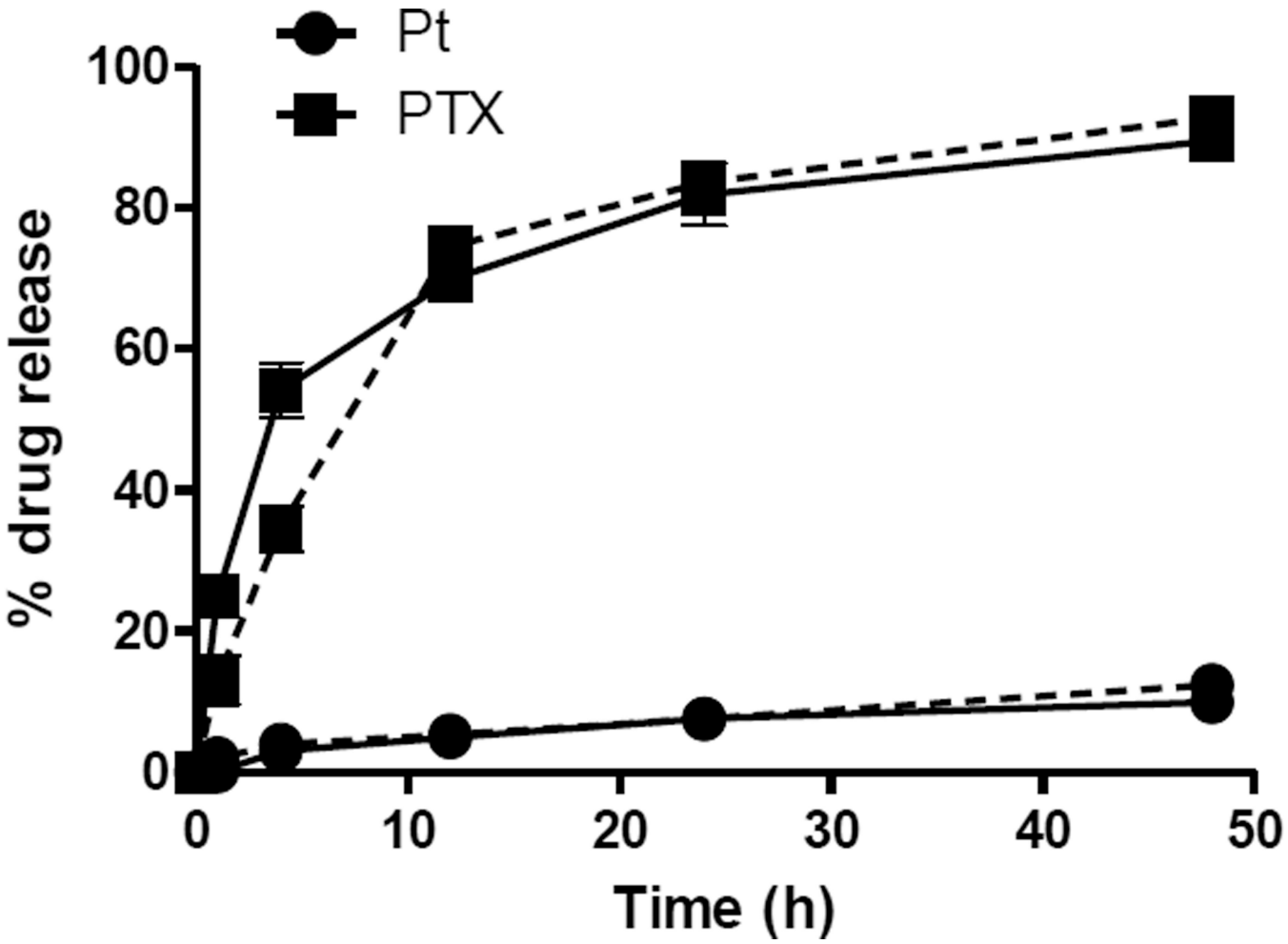

Figure 2.

Drug release profiles from FA-(CDDP+PTX)/NG (solid line) and (CDDP+PTX)/NG (dotted line) for Pt (●) and PTX (■) in PBS buffer, pH 7.4. The data represent averaged values and standard deviations calculated based on three independent experiments.

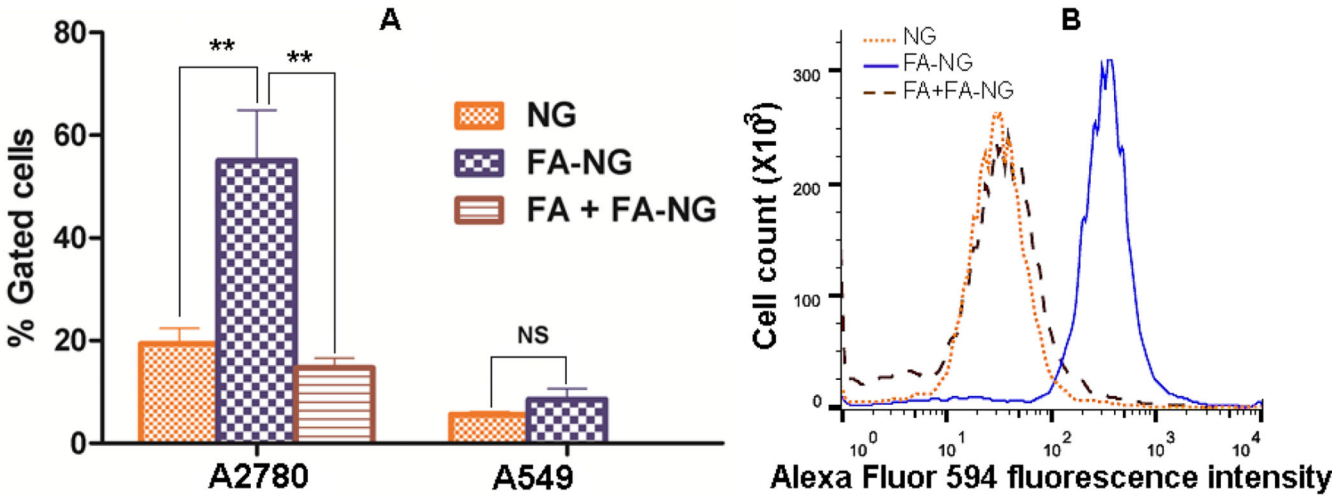

Figure 3.

A) Cellular association of Alexa fluor 594-labeled NG, FA-NG and FA-NG in presence of free FA in FR+ A2780 and FR− A549 cell lines at 30 min. B) Inhibitory effect of free FA on the cellular association of FA-NG in FR+ A2780 as analyzed by flow cytometry. FA-NG = 0.5 mg/mL and 0.2 μmol FA/mg polymer. [FA-NG] = 0.5 mg/mL and 0.2 μmol folate/mg polymer. ** indicate significantly higher uptake of FA-NG vs. NG and FA-NG in presence of free FA. ** $P < 0.01$ and ^{NS} not significant. Data are mean ± SD (n = 3).

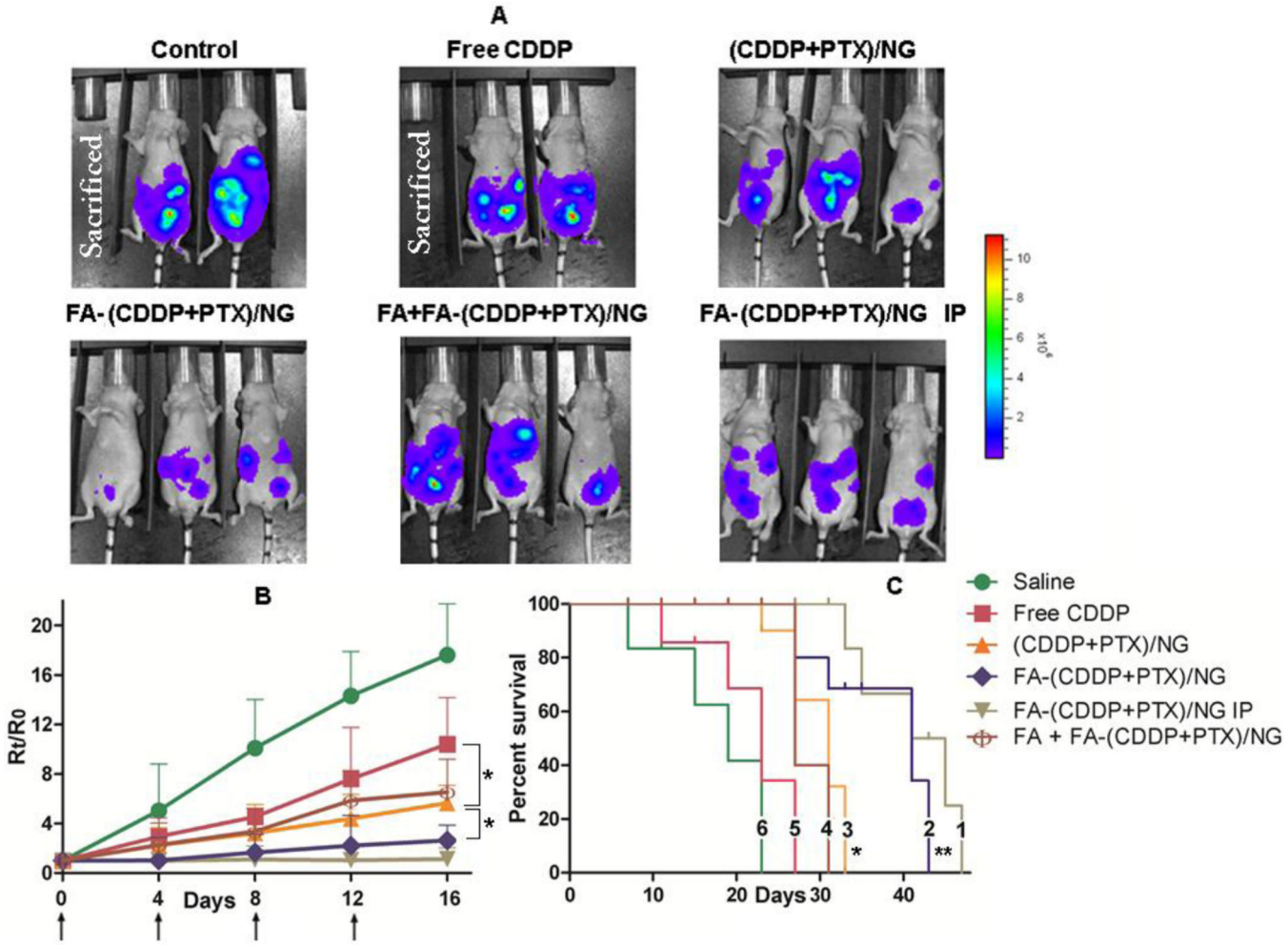

Figure 4.

In vivo antitumor efficacy of FA-(CDDP+PTX)/NG in A2780/Luc human ovarian cancer xenograft-bearing female nude mice. (**A**) Bioluminescence images of each 3 mice representative for 8 mice per experimental arm after treatment (day 16). The colored scale bar indicates the intensities of bioluminescence in photons/s/cm^2/sr. (**B**) Comparison of tumor growth inhibition following IV administration of FA-(CDDP+PTX)/NG (◆) or (CDDP+PTX)/NG (▲) or mixture of 1 mg/kg FA and FA-(CDDP+PTX)/NG (φ) or free CDDP (■) or 5% dextrose (control) (●). We used one additional group which received IP injection of FA-(CDDP+PTX)/NG (▼). Drug formulations were injected in100 μL at a dose of 4 mg CDDP or 1mg PTX equivalents/kg body weight 4 times at 4-day intervals as indicated by the arrows. Data presented in terms of relative bioluminescence units (Rt/Ro) to the day when treatment was initiated for individual animal. Values indicated are means ± SD (n = 8), **P* < 0.05. (**C**) Kaplan–Meier analysis of overall survival in FA-(CDDP+PTX)/NG IP group (1) or FA-(CDDP+PTX)/NG IV group (2) or (CDDP+PTX)/NG (3) or FA + FA−(CDDP+PTX)/NG (4) or free CDDP (5) or control group (6). Log-rank test was used to determine statistical difference between (CDDP+PTX)/NG and free CDDP groups, **P* < 0.05, and between FA-(CDDP+PTX)/NG and (CDDP+PTX)/NG groups, ***P* < 0.01.

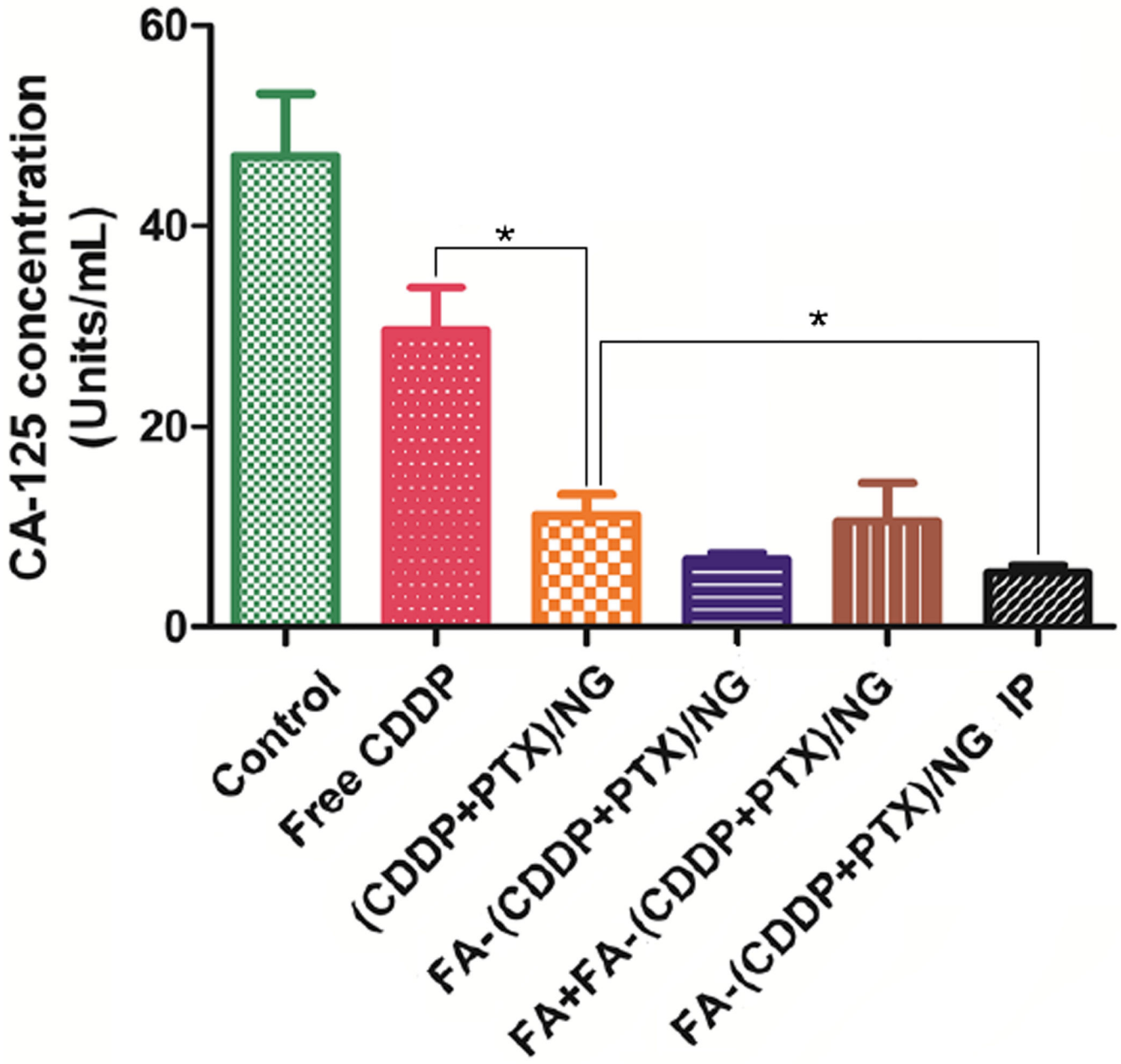

Figure 5.
CA-125 ELISA assay. Quantification of serum CA-125 levels in mice from various treatment groups. Data are presented as mean ± SD (n = 3).

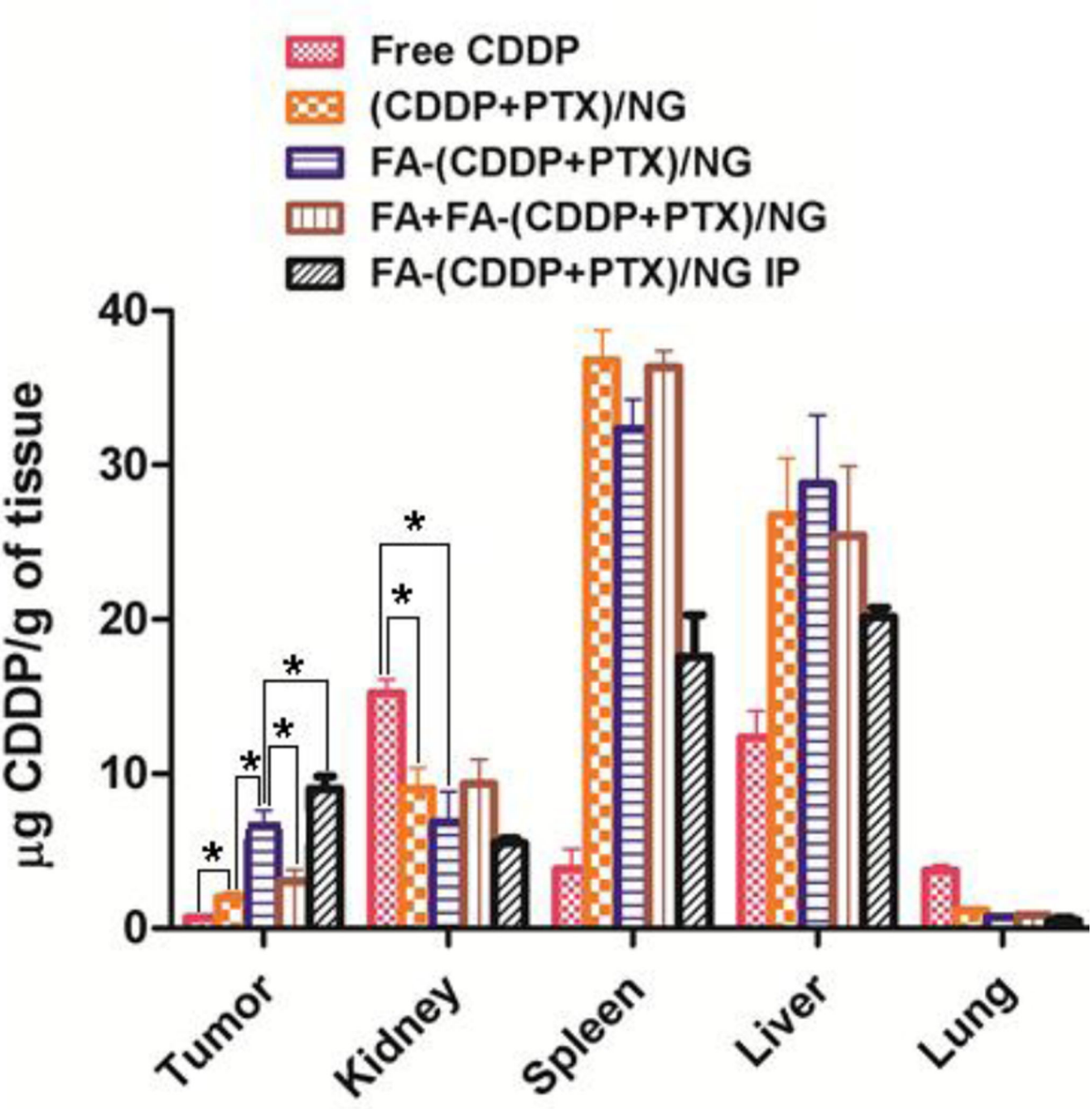

Figure 6.

Tissue distribution of platinum in different treatment groups as determined by ICP-MS. Mice were sacrificed at day 14 of the treatment with FA-[(CDDP+PTX)/NG] IP or FA-[(CDDP+PTX)/NG] or FA+ FA-[(CDDP+PTX)/NG] or (CDDP+PTX)/NG or free CDDP. Data are presented as mean ± SD (n = 3). * $P < 0.05$.

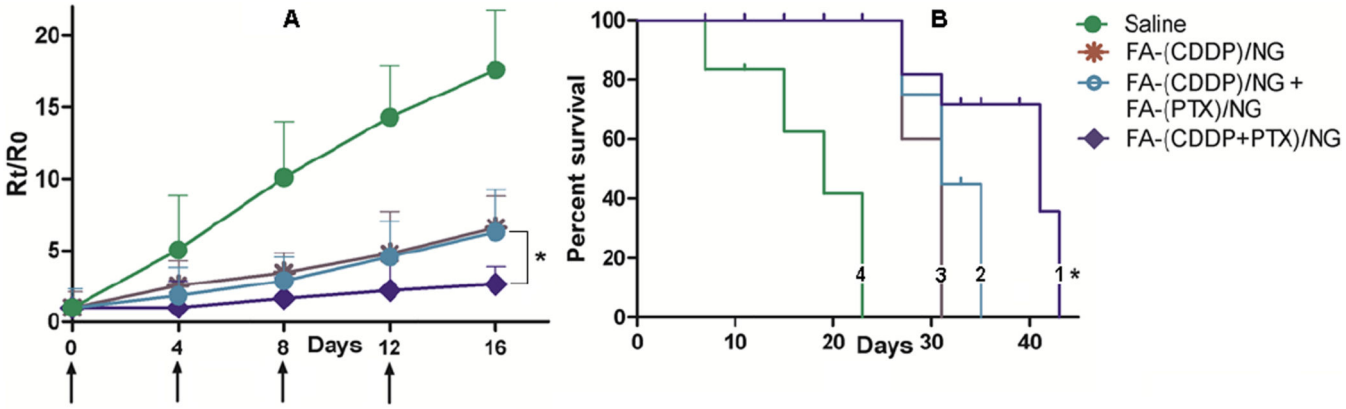

Figure 7.

In vivo antitumor efficacy of FA-(CDDP+PTX)/NG vs. FA-(CDDP)/NG + FA-(PTX)/NG co-administration against A2780/Luc human ovarian cancer xenografts. (**A**) Comparison of tumor growth inhibition as indicated by relative radiance units over time following IV administration of FA-(CDDP+PTX)/NG (◆) or FA-CDDP/NG + FA-PTX/NG or FA-(CDDP)/NG (Ж) or control (●). Drug formulations were injected in 100 μL at a dose of 4 mg CDDP or 1 mg PTX equivalents/kg body weight 4 times at 4-day intervals as indicated by the arrows. Values indicated are means ± SD (n=8). (**C**) Kaplan–Meier analysis of overall survival in FA-(CDDP+PTX)/NG (1) or FA-(CDDP)/NG + FA-(PTX)/NG group (2) or FA-(CDDP)/NG (3) or control group (4). * $P < 0.05$. Log-rank test was used to determine statistical difference between FA-(CDDP+PTX)/NG and FA-(CDDP)/NG + FA-(PTX)/NG groups, *$P < 0.05$.

Table 1

Treatment groups and drug doses used and the doses used in antitumor actificay studies.

Treatment group	Route of administration	CDDP (mg/kg)	PTX (mg/kg)	Free FA (mg/kg)
Control	IV	-	-	-
Free CDDP	IV	4	-	-
(CDDP+PTX)/NG	IV	4	1	-
FA-(CDDP)/NG	IV	4	-	-
FA-(CDDP)/NG + FA-(PTX)/NG	IV	4	1	-
FA-(CDDP+PTX)/NG	IV	4	1	-
FA + FA-(CDDP+PTX)/NG	IV	4	1	1
FA-(CDDP+PTX)/NG	IP	4	1	-

Table 2

Physicochemical characteristics of drug-loaded NGs.

Sample	D_{eff} (nm)[a]	PDIa	ζ-potential (mV)[a]	CDDP:PTX (wt/wt)
(CDDP+PTX)/NG	86 ± 2	0.26	−7.0 ± 0.7	3.84:1
FA-(CDDP+PTX)/NG	95 ± 3	0.24	−5.5 ± 1.0	3.78:1
FA-(CDDP+PTX)/NG[b]	96 ± 4	0.25	−5.7 ± 2.7	-

[a] Effective diameter (D_{eff}), polydispersity index (PDI) and ζ-potential were determined in water (pH 6.5). Data are expressed as mean ± SD (n = 3).

[b] Effective diameter, polydispersity index and ζ-potential after one month of storage in aqueous dispersion at 4°C.

Table 3

Comparison of IC_{50} values for targeted and nontargeted drug-loaded NGs against A2780 cells as determined by the MTT assay.

	IC_{50} (μM)[a]	
	24 h	**48 h**
(CDDP+PTX)/NG	3.0 ±1.3	0.4 ± 0.1
FA-[(CDDP+PTX)/NG]	1.4 ± 0.7	0.3 ± 0.1

[a] Calculated with respect to CDDP.